Spring 2017

Flooding and Inundation Modeling in the Great Bay Estuary

Anna E. Simpson
University of New Hampshire, Durham, aet96@wildcats.unh.edu

Flooding and Inundation Modeling in the Great Bay Estuary

By

Anna Simpson

Advisor: Thomas Lippmann

Honors Thesis

Submitted to the Department of Earth Sciences
In Partial Fulfillment of the Requirements for the Degree of
Bachelor of Science in Earth Science: Oceanography
at the
University of New Hampshire

May 2017

Table of Contents

List of Figures

Abstract

As part of this research, FVCOM, a finite-volume coastal ocean numerical hydrodynamic model (Chen, *et al.*, 2003), was implemented into the Great Bay estuary. FVCOM is one of several community models that have been developed for coastal regions, and was selected because it utilizes an unstructured grid to discretize the model domain. The unstructured grid provides the ability to have fine scale resolution near the boundary or coastline and decreased resolution away from the boundary where the flow field is less complicated, resulting in greatly reduced computational expense in less dynamic regions allowing model runs to be completed in much shorter time periods. Grid development also requires that bathymetric data is accurately assigned to grid nodes in such a way that the model itself will be numerically stable. This requires significant development time implementing an appropriate grid mesh (Persson and Strang, 2004) with bathymetry data that has been smoothed to limit inherent numerical noise in the computations. FVCOM was implemented on a grid with finest resolution equaling 30 m, and then tested on a 10 day run with offshore forcing determined analytically by the 8 most energetic semi-diurnal (M2, N2, S2, K2) and diurnal (K1, O1, P1, Q1) tidal constituents at Fort Pt., NH (https://tidesandcurrents.noaa.gov/harcon.html?id=8423898), and including fresh water river fluxes from 6 rivers equivalent to 5 times the average daily discharge (Ward and Bub, 2007). The model was further tested utilizing the 100 year tropical storm event estimated from the North Atlantic Coast Comprehensive Study (NACCS; USACE, 2015), and the highest projected sea level rise scenario for year 2100 estimated by NOAA (http://www.corpsclimate.us/ccaceslcurves.cfm). The numerically stable model indicates that the grid can be used to simulate tidal forcing with maximum projected year storm surge and sea level rise in the Great Bay, and – with further development to include finer (10 m) mesh resolution and inclusion of surface waves and wind forcing – may be able to predict future flooding scenarios based on forecasted storm events and sea level rise.

Introduction

Numerical models are used to study complex hydrodynamic systems that are often too difficult or time-consuming to observe with field observations. These models solve governing equations where high computing power is required to adequately resolve details of the flow and transport. Hydrodynamic models for a coastal system give outputs of a variety of variables including sea surface elevation, current velocity, bed stress, temperature, and salinity. The models can be used to simulate waves, tides, wind-driven currents, and water levels, and subsequently predict flooding and inundation scenarios that are associated with various storm events and sea level rise. Understanding the effect of flooding and inundation in the Great Bay estuary is of particular interest in New Hampshire because of high density land use practices and the proximity of people living near its borders that are at risk from future sea level rise and increased storm intensity induced by a changing climate. In this work we focus on the hydrodynamic component, and will not include testing of wave or atmospheric models.

The numerical solutions for a hydrodynamic model are governed by the equations of conservation of mass and momentum in a fluid. These mathematical formulations are broken down into discrete calculations that computers can solve through implementation of numerical algorithms. FVCOM solves the primitive equations of motion (Chen, *et al.*, 2003) given by

$$\frac{\partial u}{\partial t} + u\frac{\partial u}{\partial x} + v\frac{\partial u}{\partial y} + w\frac{\partial u}{\partial z} - fv = -\frac{1}{\rho_o}\frac{\partial (p_H + p_a)}{\partial x} - \frac{1}{\rho_o}\frac{\partial q}{\partial x} + \frac{\partial}{\partial z}\left(A_z\frac{\partial u}{\partial z}\right) + F_u \quad (1)$$

$$\frac{\partial v}{\partial t} + u\frac{\partial v}{\partial x} + v\frac{\partial v}{\partial y} + w\frac{\partial w}{\partial z} - fu = -\frac{1}{\rho_o}\frac{\partial (p_H + p_a)}{\partial y} - \frac{1}{\rho_o}\frac{\partial q}{\partial y} + \frac{\partial}{\partial z}\left(A_z\frac{\partial v}{\partial z}\right) + F_v \quad (2)$$

$$\frac{\partial w}{\partial t} + u\frac{\partial w}{\partial x} + v\frac{\partial w}{\partial y} + w\frac{\partial w}{\partial z} = -\frac{1}{\rho_o}\frac{\partial q}{\partial z} + \frac{\partial}{\partial z}\left(K_m\frac{\partial w}{\partial z}\right) + F_w \quad (3)$$

$$\frac{\partial u}{\partial x} + u\frac{\partial v}{\partial y} + \frac{\partial w}{\partial z} = 0 \quad (4)$$

where x, y, z are the east, north and vertical axes and corresponding velocity components are u, v, and z, ρ is density, p_a is air pressure at sea surface, p_H is hydrostatic pressure, q is the non-hydrostatic pressure component, f is Coriolis parameter, g is the gravitational acceleration, A_z and K_m are the vertical eddy viscosity coefficients, and F_u, F_v, and F_w are external forcing functions.

The total pressure is given by the sum of the hydrostatic pressure, atmospheric pressure, and the non-hydrostatic contribution, and can be defined as

$$\frac{\partial p_H}{\partial z} = -\rho g \implies p_H = \rho_o g\zeta + g\int_z^0 \rho dz' \tag{5}$$

In order to solve (1)-(4), boundary conditions must be specified at the surface and the bottom. The surface and bottom boundary conditions are given by

$$K_m\left(\frac{\partial u}{\partial z}, \frac{\partial v}{\partial z}\right) = \frac{1}{\rho_o}\left(\tau_{sx}, \tau_{sy}\right), w = \frac{\partial \zeta}{\partial t} + u\frac{\partial \zeta}{\partial x} + v\frac{\partial \zeta}{\partial y} + \frac{E-P}{\rho}, \quad at\ z = \zeta(x, y, t) \tag{6}$$

$$K_m\left(\frac{\partial u}{\partial z}, \frac{\partial v}{\partial z}\right) = \frac{1}{\rho_o}\left(\tau_{bx}, \tau_{by}\right), w = -u\frac{\partial H}{\partial x} - v\frac{\partial H}{\partial y} + \frac{Q_b}{\Omega}, \quad at\ z = -H(x, y)$$

where the stresses for surface wind and the bottom in the *x* and *y* components are (τ_{sx}, τ_{sy}) and $\left(\tau_{bx}, \tau_{by}\right) = C_d\sqrt{u^2 + v^2}(u, v)$, groundwater flux is Q_b, and groundwater source is given by Ω (note that groundwater is not considered in the present work).

The bottom drag coefficient, C_d, is determined by a logarithmic bottom boundary layer assuming no motion at the sea floor,

$$C_d = \max\left(\frac{k^2}{\ln\left(\frac{z_{ab}}{z_o}\right)^2}, 0.0025\right) \tag{7}$$

where the von Karman coefficient, $k = 0.4$ and the bottom roughness parameter is z_o.

In FVCOM, the governing equations, (1)-(4), are solved using a generalized terrain-following ("sigma" or σ) coordinate system in which the vertical coordinates are normalized to range from the bottom, z =-1, to the surface, z = 0 (Mellor and Blumberg, 1985). A schematic of the sigma coordinate system is shown in Figure 1. In this so-called sigma coordinate system, the horizontal diffusion terms are defined as

$$DF_x \approx \frac{\partial}{\partial x}\left[2A_m H\frac{\partial u}{\partial x}\right] + \frac{\partial}{\partial y}\left[A_m H\left(\frac{\partial u}{\partial y} + \frac{\partial v}{\partial x}\right)\right] \tag{8}$$

$$DF_y \approx \frac{\partial}{\partial x}\left[A_m H\left(\frac{\partial u}{\partial y} + \frac{\partial v}{\partial x}\right)\right] + \frac{\partial}{\partial y}\left[2A_m H\frac{\partial v}{\partial y}\right] \tag{9}$$

where A_m and A_h are the eddy diffusion coefficients and H is the water depth. The horizontal eddy and thermal diffusion coefficients are simplified to correctly simulate the 1-D bottom boundary layer. The assumption is made that horizontal diffusion occurs parallel to the σ-layers and are necessary for the current stability and validity of FVCOM.

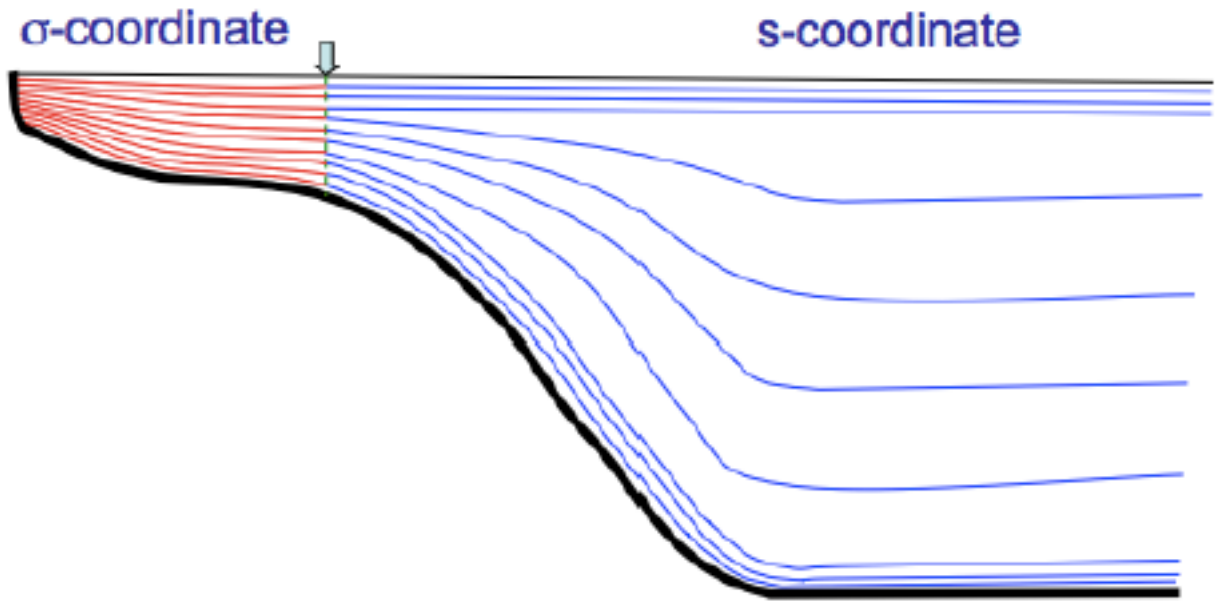

Figure 1. Schematic illustrating the sigma coordinate system with vertical layers determined by defined fractions of the total water depth. Also shown is the *s*-coordinate system further offshore which has vertical layer resolution higher near the surface and bottom that varies with depth. (taken from Chen, *et al.*, 2013)

The governing momentum and continuity equations, (1)-(4), are generally not solved at fine enough scales to resolve all motions including turbulence fluctuations, and are thus not mathematically closed unless sub-grid resolution fluid motions are parameterized and appropriate diffusion formulations are specified. In FVCOM, the Smagorinsky (1963) formulation for horizontal momentum is used, and given by

$$A_m = 0.5\,\Omega^u \sqrt{\left(\frac{\partial u}{\partial x}\right)^2 + 0.5\,\left(\frac{\partial v}{\partial x} + \frac{\partial u}{\partial y}\right)^2 + \left(\frac{\partial v}{\partial y}\right)^2} \qquad (10)$$

where Ω^u is the area of the individual momentum control element. The Mellor and Yamada (1982) level 2.5 turbulent closure model is used to describe the vertical diffusion, and determined by a specification of a vertical eddy viscosity, K_m, and solving equations for the turbulent kinetic energy with defined turbulent macroscale.

Finite volume Discretization

FVCOM discretizes the model domain into non-overlapping discrete unstructured triangular cells. A single cell (or triangle) consists of three nodes at the vertices of three sides, and a centroid. All calculations of velocities are at centroids determined by the net flux across the three sides of the cells. All scalar variables (sea surface elevation, depths, salinity, temperature, density, and diffusion coefficients) are at nodes and determined by a net flux through cross-sections between centroids and the mid-points of adjacent sides. Figure 2 illustrates the design and locations of variables in terms of cells, nodes, and centroids.

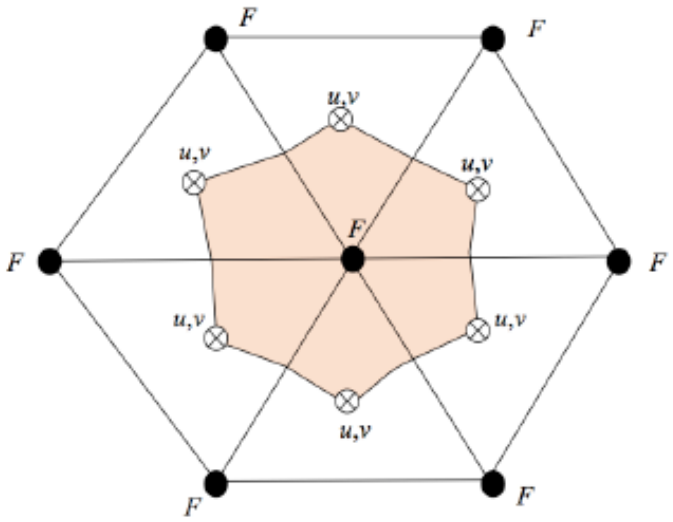

Figure 2. Schematic showing unstructured triangular grid and location of variables relative to nodes (•), centroids (⊗), and sides of cells. Variables at nodes: H, ς, ω, D, s, ϑ, q^2, q^2l, A_m, K_h; at centroids: u, v. (taken from Chen, *et al.*, 2013)

Vertical velocities, *w*, and turbulence variables are computed at the vertical interfaces between vertically stacked cells in the σ-coordinate system. All other variables (horizontal velocities and scalars) are located at the mid-level of each sigma layer. Figure 3 provides an illustration of the vertical variation in variable locations in the vertical.

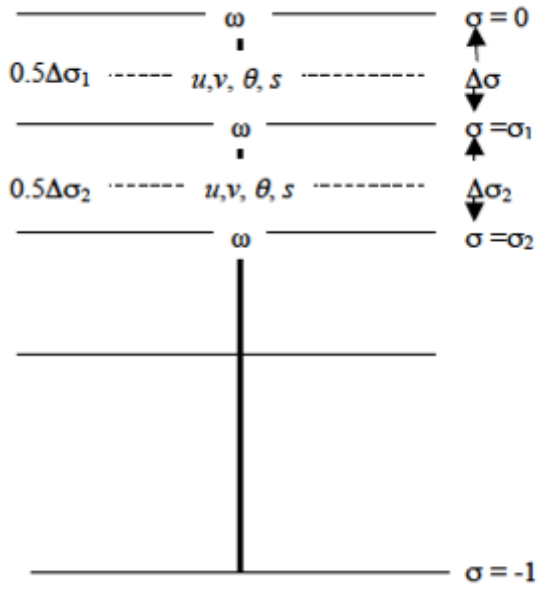

Figure 3. Schematic of vertical sigma-coordinate system. Locations of model variables: *u*, *v*, θ, *s*, ω. (taken from Chen, *et al.*, 2013)

Finite volume methods solve the equations using a "mode-split" algorithm which first solves the two-dimensional barotropic (or external) mode based on vertical integration of the velocities over the vertical domain using a fourth-order Runge-Kutta time-stepping scheme. Secondly, the three-dimensional velocities are solved with a combined explicit and implicit scheme, typically at coarser temporal resolution (because internal modes propagate at slower phase speeds than barotropic modes). Local and advection velocities are integrated using an upwind scheme accurate to second order (following Kobayashi, *et al.*, 1999). The vertical velocity is solved implicitly, requiring solutions based on forward projecting velocities to the next time step.

In our work, we have interest in simulating the flooding and inundation of ocean water owing to storm surge and projected sea level rise from climate change forecast scenarios. In order to model the movement of water onto dry land, algorithms need to be implemented that

distinguish between wet and dry cells. This is done in FVCOM through calculation of water depths at the boundary between land and water, and setting a threshold depth level for defining when cells are wet (for example, setting the criteria for dry land as water depths less than 0.05 *m*). This method is widely used in estuarine numerical models (e.g., Leendertse, 1970, 1987; Flather and Heaps, 1975; Ip, *et al.*, 1998; Zheng, *et al.*, 2003) and described in detail for FVCOM in Chen, *et al.* (2003).

External Forcing

The model can be driven by a variety of external forcing sources, including tidal and subtidal fluctuations, and river discharges. Additional forcing mechanisms such as atmospheric wind stress, heat flux, precipitation and evaporation, groundwater flux and surface gravity waves can be included but are not presently considered herein.

Forcing of water levels are included at offshore boundary nodes defined within the boundary mesh. Forcing functions can be defined analytically or with input time series from observation or other larger scale (regional) model output. Tidal elevations can be accurately defined by including the major tidal constituent amplitudes and phases for the locations at the seaward boundary. Tides can be analytically defined within FVCOM itself, or computed in other custom computer codes (*e.g.*, MATLAB) in which output surface elevation time series are created in NETCDF format for input into the model. The method for computing time series is useful because it is conducive to importing data from other models or from field observations. In particular, subtidal sea surface fluctuations due to atmospheric pressure variations (*i.e.,* storm surge) are easily included in the forcing time series.

River discharges can be specified at boundary cell edges at specific locations where fresh water tributaries flow into the Great Bay. There are six significant rivers that flow into the Great Bay estuary: the Squamscott, Lamprey, Oyster, Bellamy, Cocheco and Salmon Falls rivers. River discharges (in m^3/s) can be specified as time series based on observations or synthetically created with MATLAB functions that produce NETCDF river discharge forcing files. These river discharges can include fresh water with salinity and temperature much different from ocean values. These discharges are distributed evenly over the sigma layers, and with FVCOM are considered in the mass and salt balance of the estuary.

Forcing functions at the offshore boundary and river cells are hyperbolically ramped up from rest and ocean values to the full forcing over 2 day periods. This ramping up of the model allows numerical instabilities to be greatly reduced and creates a smooth transition from an estuary with no motion to fully modeled flow fields.

Model Domain Grid Mesh

Numerical models use a grid mesh, which separates the domain into different discretized components. The mesh resolution is important because it effects the level of detail at which the physical processes can be resolved. The ranges of scale for any grid size have tradeoffs pertaining to computational time, resolution, and model stability. The complexity of a coastline requires a finer resolution to resolve the variability of the flow while further from the shore, where the dynamics are a result of larger scale processes, the grid cells can be much larger. In an estuarine system, the goal is to achieve a stable model at 10-30 *m* grid resolution. Two types of grids are typically used in numerical models.

In a rectilinear/orthogonal grid, also referred to as a structured grid, quadrilateral cells define the mesh, and are advantageous because numerical finite difference algorithms are straightforward and efficient. The disadvantages to this type of grid are the resolution flexibility and potential for wasted computational time. Along a complex coastline, the same resolution occurs at the shoreline as in regions far from shore. If a fine resolution is chosen, which is often desired in order to resolve high complexities in shallower water, computational time will be expended further away from the coast where flows are more uniform. This greatly reduces computational efficiency which could be eliminated by using a larger grid size in the less complex area. Thus, there is a tradeoff between fine resolution near the coastline and computational efficiency. A compromise between these two opposing facets can be achieved, for example, by nesting finer grid cells in regions of high complexity or interest within a larger domain with larger grid cells.

Unstructured grids provide the grid resolution flexibility that is inherently advantageous in resolving issues with computation efficiency for model domains with finer resolution along the coastline and in shallow water and coarser resolution further away from the coastline. An unstructured grid is composed of triangular cells which allow for smooth transition between fine resolution near the coastline or other areas where finer resolution is needed and coarser

resolution far from those areas. Overall, unstructured grids reduce the number of required calculations, and therefore the computational time needed to solve the numerical equations. Moreover, they can be easily modified to follow a complex boundary without creating domain cells in unneeded regions.

Methods

Grid Generation

A shoreline file is created to define the boundary for the grid generator. The minimum and maximum element sizes must be taken into consideration when the boundary points are determined by the algorithm. If the element sizes at the coast are equal to or smaller than the points making up the coastline, the meshing algorithm does not have a problem creating a high-quality mesh. If the element sizes are larger than the distance between the coastline points, issues in quality and convergence occur. The coastline is recreated using an algorithm which results in an accurate representation of the coastline with the appropriate number of vertices. For the Great Bay grid mesh, the topographic contour 8 *m* above mean sea level was used to define the boundary limits, thereby accommodating the largest expected sea level inundation from simulations with maximum storm surge and sea level rise.

The mesh algorithms used to generate the grid are based on a simplex mesh and truss structure developed within a few dozen lines of MALAB code (Distmesh.m; Persson and Strang, 2004). A signed distance function creates a negative value inside the region, and is important in representing the geometry. It is also used to repetitively find the distance to the closest point at a nodal point. Meshpoints (nodes) of the truss and a force-displacement function is applied for each iteration and equilibrium is solved. The Delaunay triangulation algorithm adjusts the edges of the triangles and the forces move the nodes. The node is determined to be inside or outside the region by the signed distance function. The outputs from Distmesh are the node positions, *p*, which contain *x*, *y* coordinates for each node, *N*, and the triangle indices, *t*, where each row has 3 integer entries that specify the node numbers that define the triangle. The inputs are a user-defined distance function , *fd*, that includes the boundary, the edge length function, *fh*, and edge length, *h0*, which defines the initial distribution of *p* and the minimum grid size desired. In uniform meshes, *fh* would be constant. The bounding box, *bbox*, defines the maximum extent of

the domain, and the parameter *pfix* defines node positions that are required to be in the final mesh. The offshore boundary nodes where the model is forced (*e.g.*, by the tides and storm surge) were selected manually, and correspond to the output save points from the Northeast Coastal Ocean Forecast System (NECOFS) that utilizes FVCOM implemented on the Gulf of Maine GOM 4 grid.

A hyperbolic tangent function was used in *fh* to create a mesh with the appropriate cell sizes, *dH*, in the regions where finer resolution is desired

$$dH = h0 + B\ dp - \frac{B}{A}\tanh\left(A\ dp\right) \tag{11}$$

where dp is the distance from any given node to the boundary. The coefficients *A* and *B* were determined through empirical iteration to yield appropriate mesh size distribution. When the nodes are close to the boundary (small *dp*), *dH* goes to *h0*. When the *Adp* gets large, *dH* goes to *h0* + *B*(*dp* – 1/*A*). Bar width *dH* as a function of *dp* for various values of *A* and *B* are shown in Figures 4 and 5 with constant *A* with *B*, respectively. Best distribution of *dH* resulted from coefficients *A* = 0.2 and *B* = 0.45. The initial bar width, *h0*, was set to 30 *m*, defining the finest scale resolution for this grid.

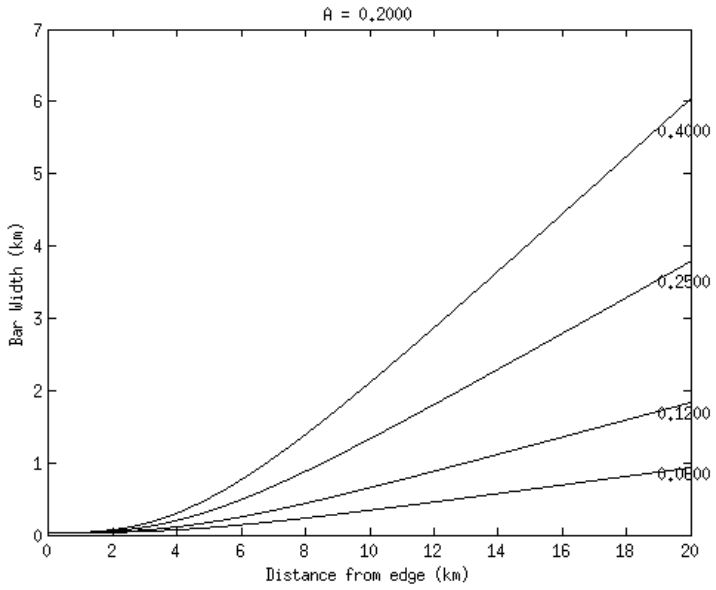

Figure 4. Bar width changes as a function of nodal distance from the boundary edge for a constant *A* = 0.2 and *B* = 0.08, 0.12, 0.25, and 0.45.

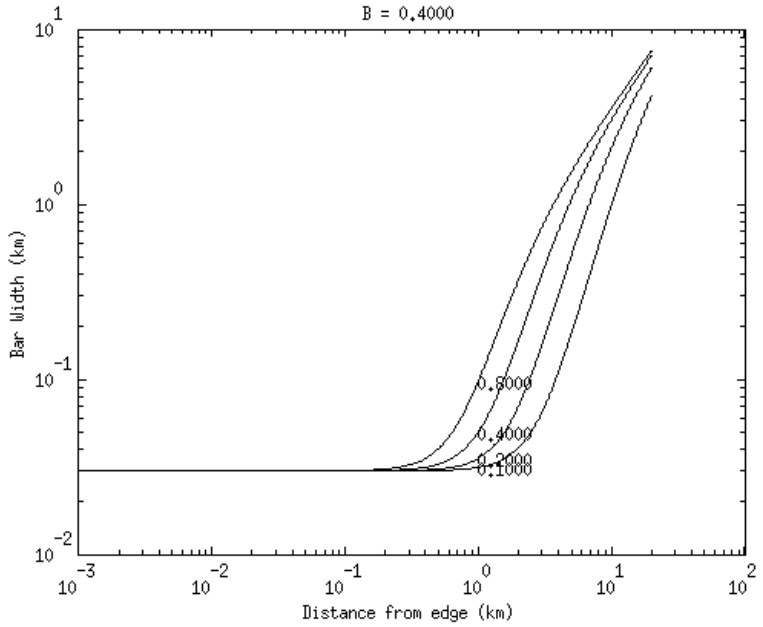

Figure 5. Bar width changes as a function of distance from the boundary edge B = 0.40 and A = 0.1, 0.2, 0.4, 0.6.

The initial grid was fixed according to user specification and 500 iterations of the distmesh2d algorithm. 'Bad' nodes and triangles were defined by not having bars attached to a node or having crossing bars. These were removed manually and through an algorithm that checked the area of triangles and length of bars and compared it to what was expected from placement of surrounding nodes. The final grid mesh is shown in Figure 6 for the whole domain, and for a closeup in Figure 7.

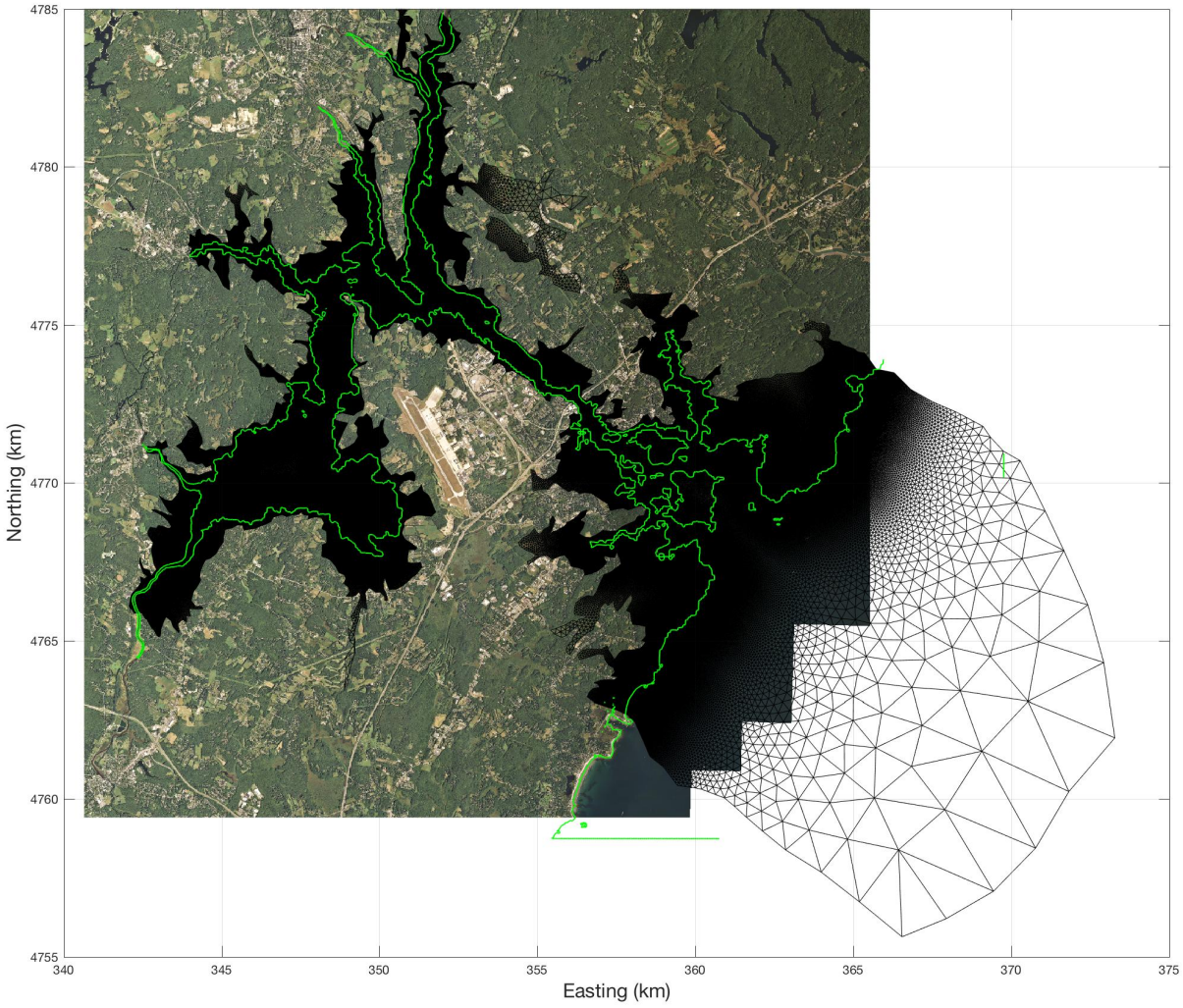

Figure 6. Final unstructured grid for the Great Bay estuary. Green line designates the shoreline at mean sea level. The outer boundary of domain is defined by the 8 *m* elevation contour. The six most seaward boundary nodes are the forcing location.

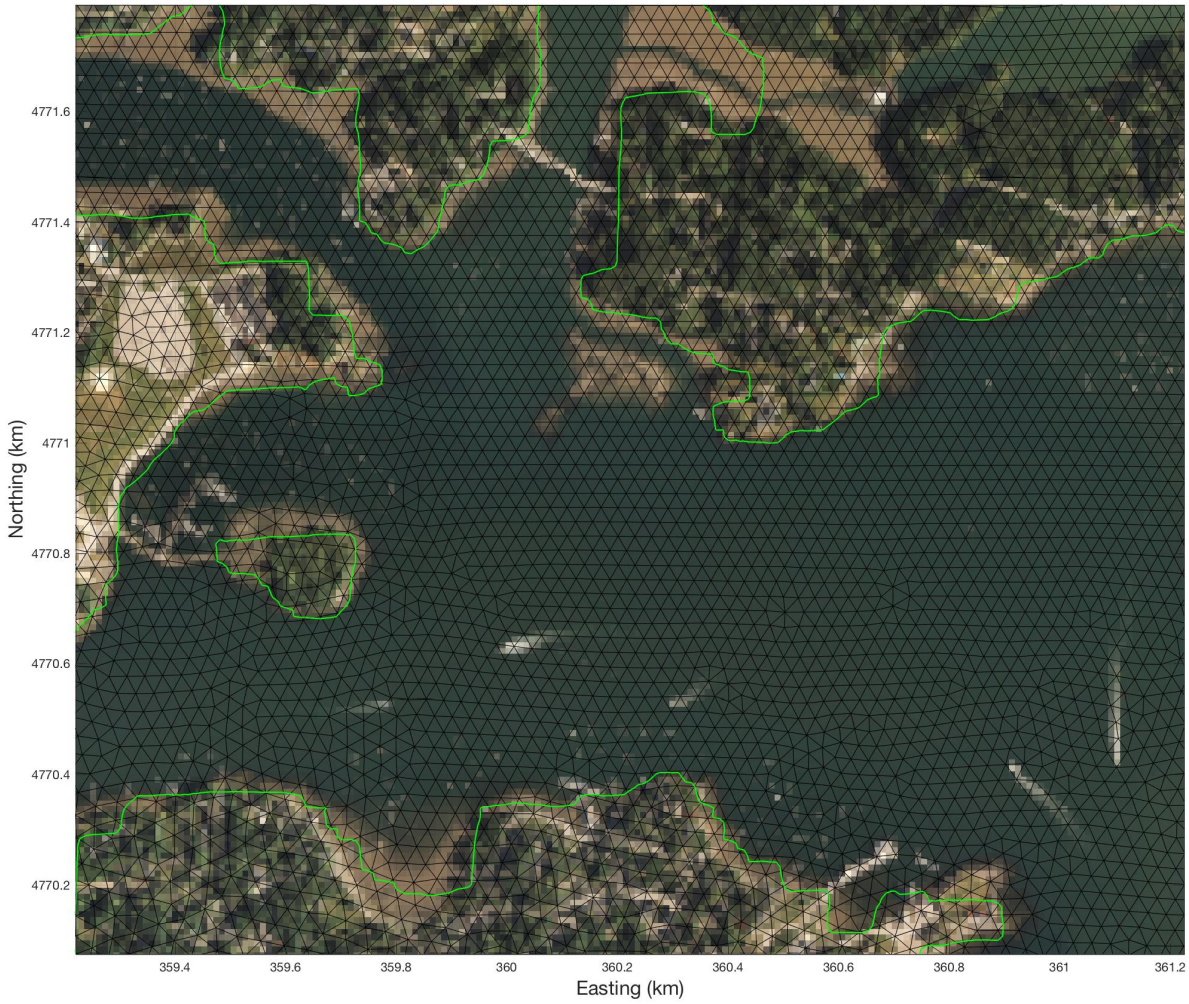

Figure 7. Close up of portion of the grid, showing fine scale resolution near boundary. The shoreline at mean sea level is shown with the green line.

Grid Bathymetry

Model grid bathymetry (Figure 8) was determined for Great Bay estuary from observations of subaerial and river topography obtained from LIDAR surveys by the USACE and USGS, and subaqueous bathymetry obtained from various hydrographic surveys conducted by JHC/CCOM at UNH, USGS, NOAA and USACE. This bathymetry was smoothed using optimal interpolation methods to reduce sharp gradients within the model (Plant, *et al.*, 2002).

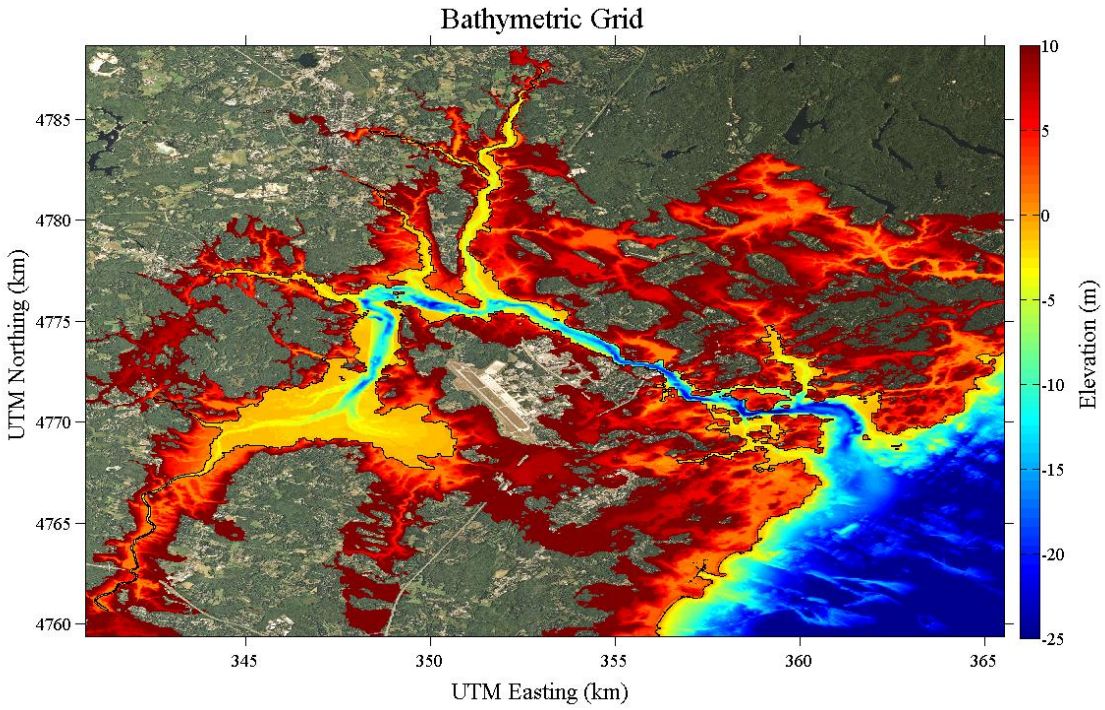

Figure 8. Bathymetric map of Great Bay estuary. Black contour designates mean sea level. The domain boundary is determined by the 8 *m* contour. Elevations are in *m* relative to mean sea level.

The depths within the model were determined by linearly interpolating the bathymetric depths onto the node points of the FVCOM unstructured grid mesh. An accurate representation of the bottom topography with approximations is necessary to ensure that the model instabilities are suppressed (*e.g.*, the smoothing of the grid). The nature of the domain must not be wildly altered to best simulate the actual flows. In FVCOM, mean sea level is at 0, with positive elevations going upwards.

Offshore Forcing

The model is forced at the offshore nodes by prescribing tidal fluctuations with the 8 most energetic semi-diurnal (M2, N2, S2, K2) and diurnal (K1, O1, P1, Q1) tidal constituents from Fort Pt., NH (https://tidesandcurrents.noaa.gov/harcon.html?id=8423898). Figure 9 shows a 30 day time series of sea surface elevation based on the prescribed amplitudes and phases of each tidal harmonic. At Fort Pt., the tides are mixed semi-diurnal with a prominent spring-neap

cycle. The starting phase is arbitrary, and chosen to best test the model for abbreviated (10 day) runs that included the highest spring tide.

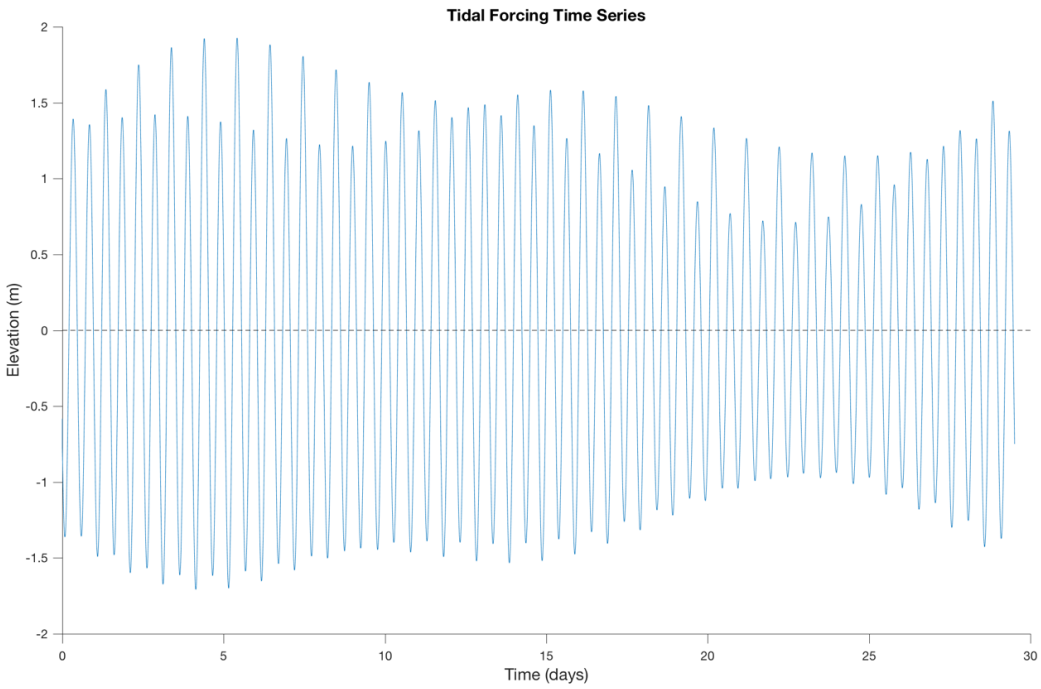

Figure 9. Tidal forcing time series

Storm surge data from simulated tropical and extratropical storms were obtained from the North Atlantic Coast Comprehensive Study (NACCS; USACE, 2015). In the NACCS study, 1100 tropical storms were simulated based on statistical approximations of conditions from recorded events over the past 100 year. Histograms of the maximum storm surge at save points near the mouth of the Piscataqua River were computed, and the storm closest to the 99% exceedance level chosen as the predicted 100 year storm event. The storm surge time series (Figure 10) was added to the tidal time series such that the maximum surge corresponded to the maximum spring tide (Figure 11). This time series thus includes the effects of a predicted 100 year storm event on flooding and inundation with maximum sea surface height that would occur at the highest spring tide. In addition, the model predicts the maximum currents expected for this event.

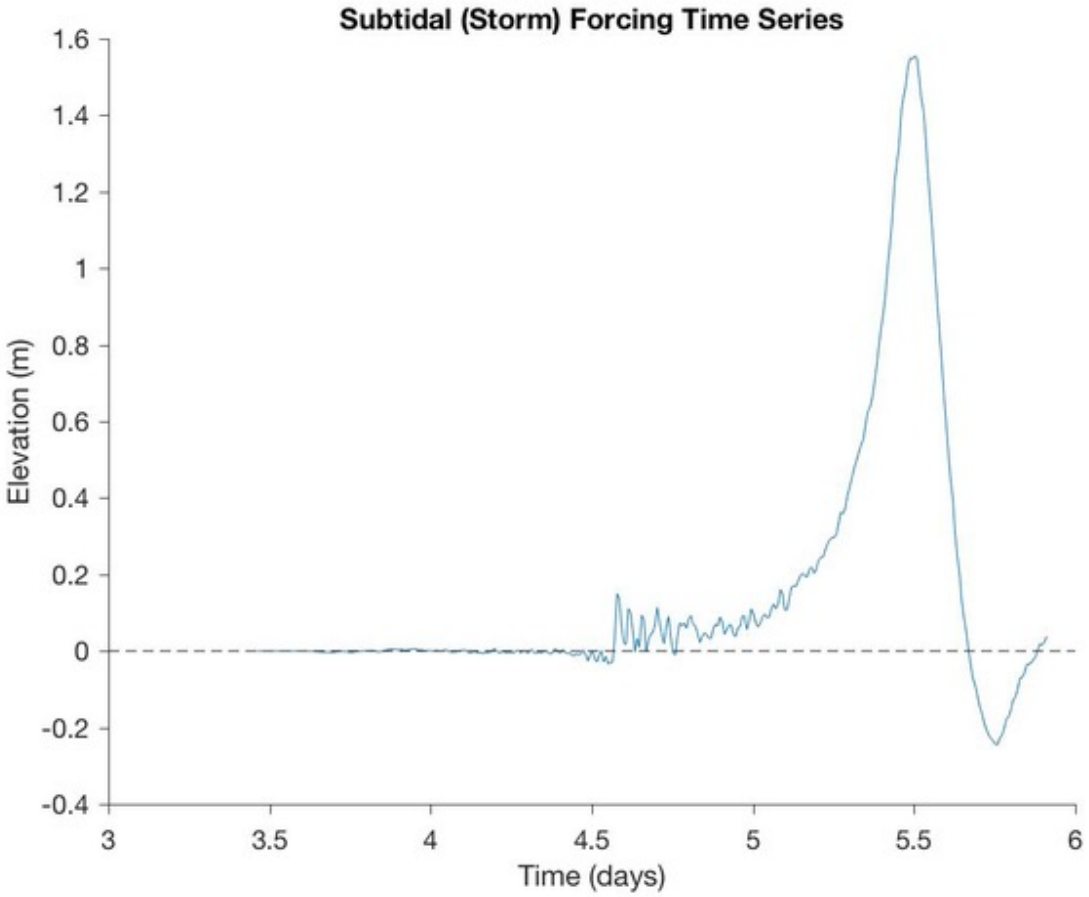

Figure 10. Storm forcing time series for the predicted 100 year tropical storm at the mouth of the Piscataqua River (from the NACCS data base).

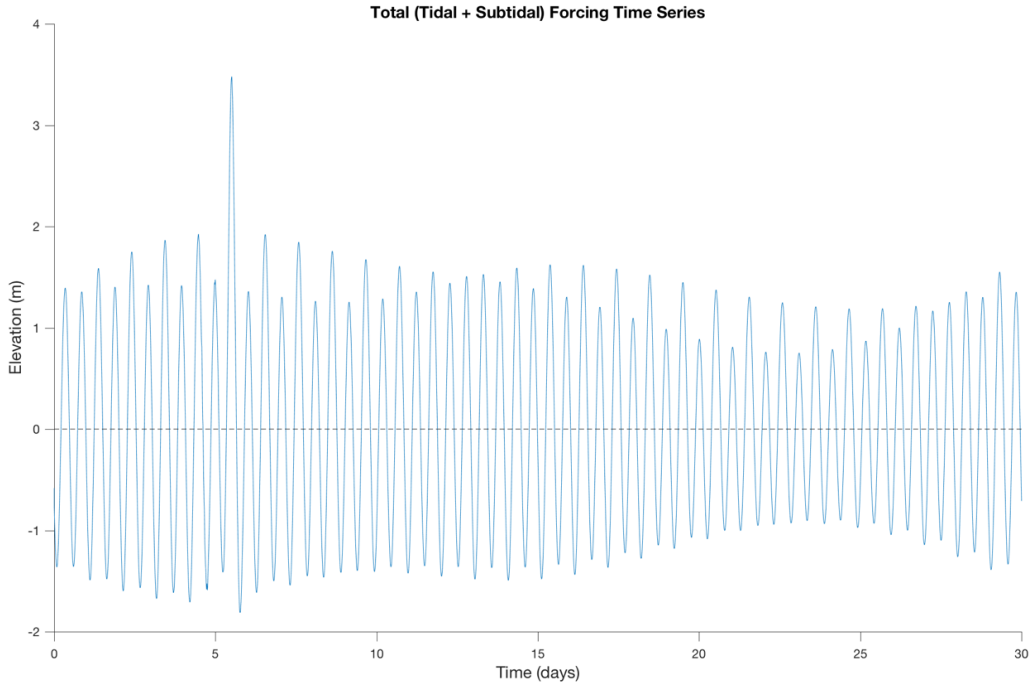

Figure 11. Forcing time series including tides and 100 year tropical storm synchronized to the maximum spring tidal excursion.

River Discharges

The location of the 6 major rivers that flow into the Great Bay estuary, the Squamscott, Lamprey, Oyster, Bellamy, Cocheco, and Salmon Falls, are shown in Figure 12. Their average daily discharges are listed in Table 1 (Ward and Bub, 2007). The fluxes can be modified in the model simulations to approximate higher discharges during high precipitation or spring-run off periods by linearly increasing the discharges by a constant factor (such as by 3 or 5 times the average annual discharge). The mixing can also be tested using temperature and salinity which differs from ocean values.

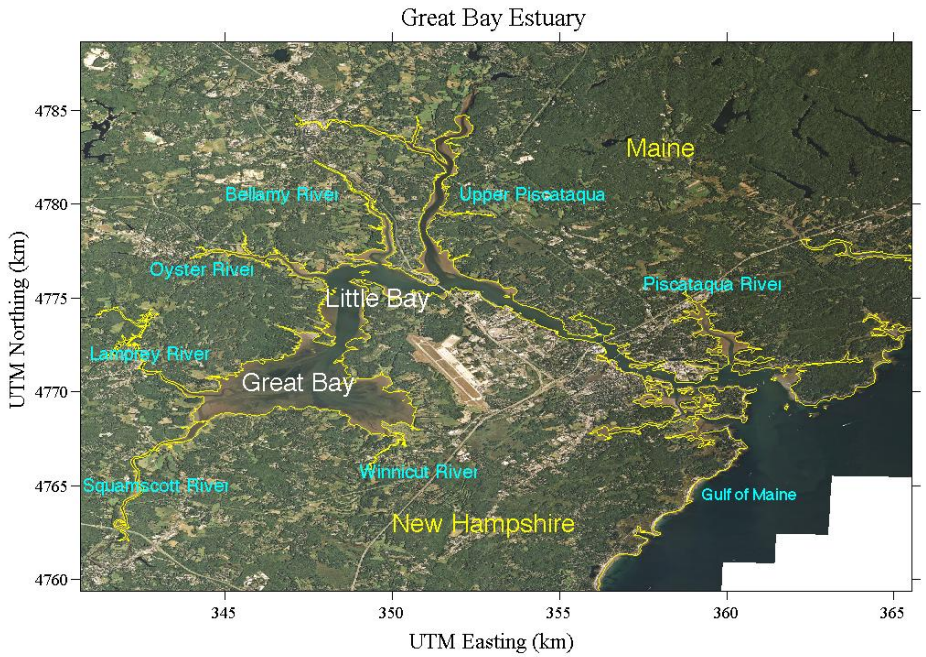

Figure 12. Image of seacoast New Hampshire taken from Google Earth with the 6 major rivers labeled. The Upper Piscataqua river includes the Cocheco and Salmon Falls rivers.

River	Discharge (m^3/s)
Squamscott	3.1
Lamprey	8.0
Oyster	0.6
Cocheco	4.7
Salamon Falls	5.4
Bellamy	1.0

Table 1. Average daily discharges (in m^3/s for the 6 major rivers flowing into the Great Bay estuary (Ward and Bub, 2007).

Sea level rise

Sea level rise projections for year 2100 were obtained from NOAA (Figure 13) (http://www.corpsclimate.us/ccaceslcurves.cfm). The highest projected curve was chosen for our

sea level rise scenario. The 2 *m* surface height was added to the 100 year storm scenario synchronized with maximum spring tide.

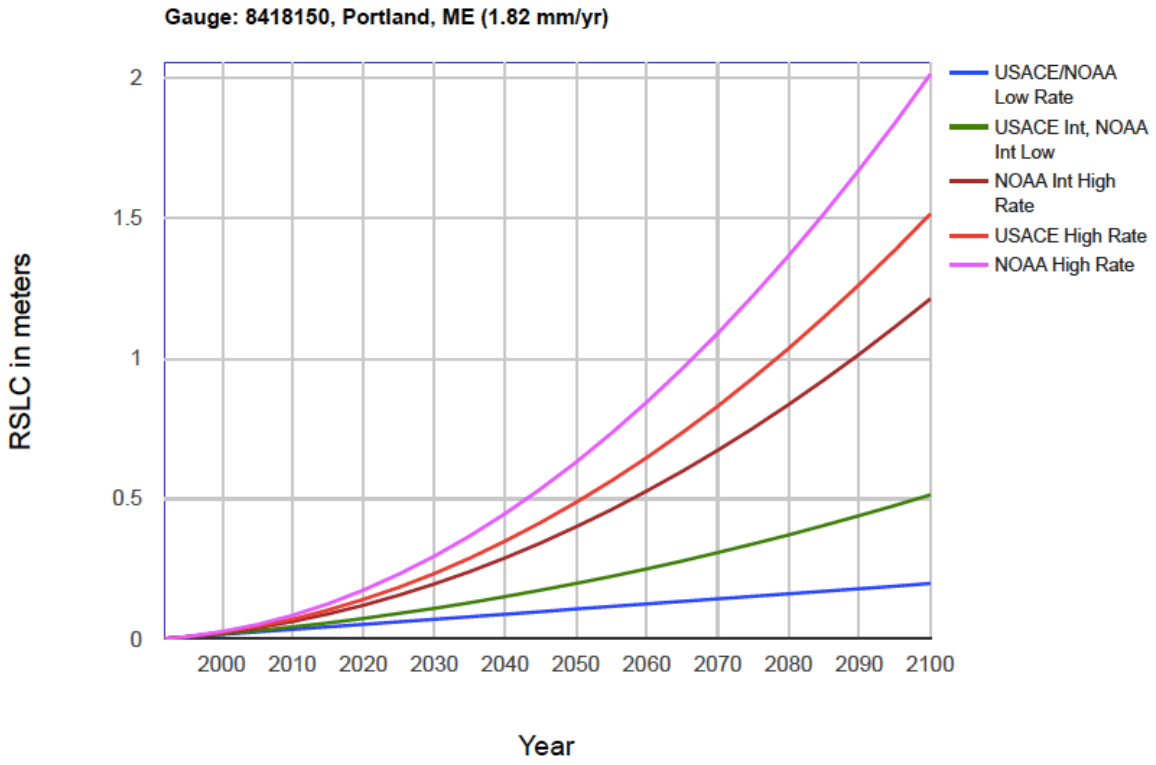

Figure 13. Estimated relative sea level change projections from 1992 to 2100 at gauge 84815, located in Portland, ME (present rate of 1.82 *mm/yr*). Different forecast models with the low, intermediate, and high estimates are shown.

Model Parameters

The turbulent coefficients used in the model equations, A_h and A_z were 1.0 m^2/s and 0.04 m^2/s, respectively. Values were determined from extensive modeling in the same estuary using the Regional Ocean Modeling System (ROMS; Cook and Lippmann, 2016). Coefficients are subject to change for the model, but must accurately represent the physics observed. The bottom roughness (z_o) used was 0.06 *m*. The mesh size ranged from 30 *m* to 2 *km*. A free surface and closed bottom defined the boundary conditions. The model spin-up was 2 days (based on a hyperbolic ramp from rest). The model time step was 0.25 *s*. The mode split method solves the barotropic 2-D model every time step and the baroclinic 3-D model every 5 time steps. The discretization over spatial, Δx, and temporal, Δt, scales adheres to the Courant-Friedrichs-Lewy

(*cfl*; Courant, *et al.*, 1928) condition such that $\frac{\Delta t}{\Delta x} * C' < 1$, where C' is the speed of the surface waves $\sqrt{gH}$ where *H* is the total water depth.

Model Simulations

Tidal Forcing with River Discharges

The FVCOM model was tested on the 30 *m* grid (178,717 nodes; 350,099 cells) with tidal forcing based on the Ft. Point tide gauge tidal constituent amplitudes and phases. River discharge was equivalent to 5 times the average daily discharge for this simulation. The spin-up time for the model was 2 days and it ran for 10 days for testing without fail on the a CRAY XE6m-200 supercomputer (Trillian) located at UNH in the Institute for Earth, Oceans, and Space (EOS) Space Science Center (http://trillian-use.sr.unh.edu/index.php/Main_Page). The model was run in parallel mode with 8 nodes, each with 32 processors (256 total processors). The three-dimensional simulation (with 10 vertical sigma layers) took less than 10 hours to complete.

The outputs included temperature, salinity, currents (*u*, *v*, *w*), sea surface elevation, wet-dry cell identification arrays, and a variety of spatially and temporally varying mixing and bottom stress variables. Model data is output at grid nodes or cells (depending on variable) at user-defined time increments (in our case on 10 *min* intervals). Data output file format is netcdf, and can easily be read into other analysis programs, such as MATLAB. Total file size was 174.6 GB. Owing to the large file size, the Trillian file system was remotely mounted to computers in the Center for Coastal and Ocean Mapping, and data transferred on demand from within custom MATLAB scripts for analysis and display.

An example model data ouput is shown in Figure 14. In this figure, the horizontal current magnitudes for the spring ebb tide for the Great Bay estuary are displayed using the wet-cell mask to blank dry cells (with water depths less than 0.05 *m*). The highest magnitudes of 1.8 *m*/*s* are located in the channel of the Piscataqua River in qualitative agreement with expected velocities based on ROMS modeling efforts (Cook and Lippmann, 2016). The shallower mudflats in the upper bay have the lowest magnitudes, as expected. Close up versions of the flood and ebb currents in Little Bay of the Great Bay estuary are shown in Figures 15 and 16, respectively. For display purposes, the number of vectors shown is decimated by a factor of 3,

and overlain on top of depth color contours. For both the flood and ebb currents, the vector length, hence the magnitude, is greater in deeper channels than the shallow mud-flats.

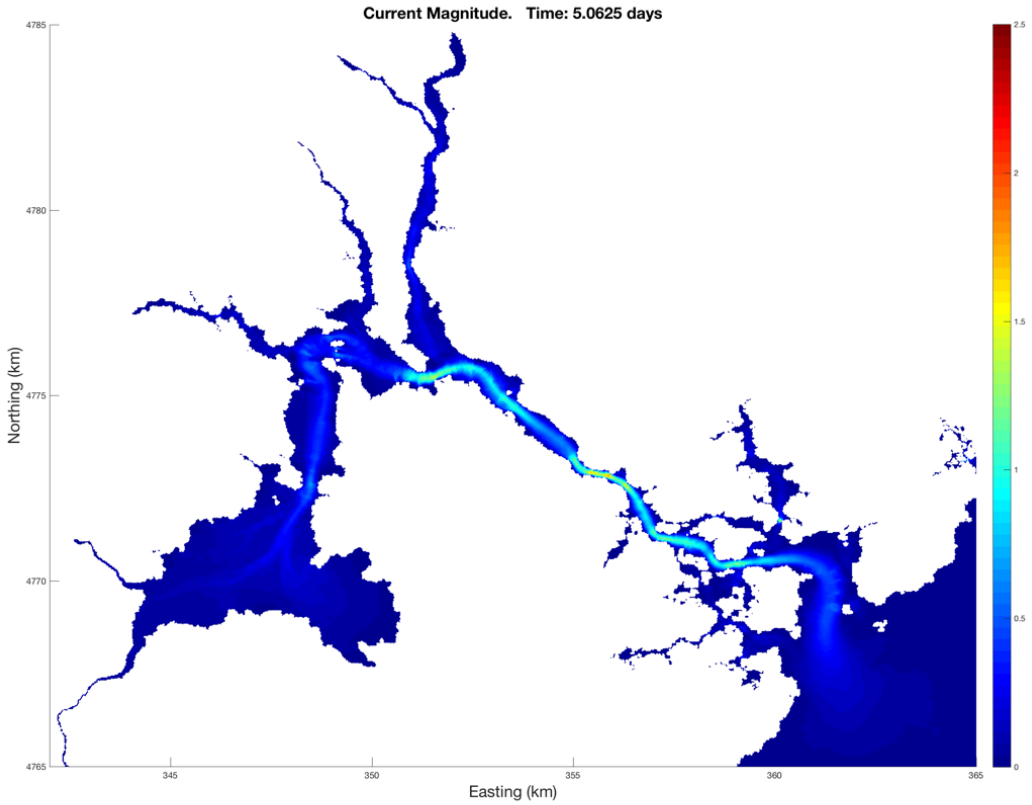

Figure 14. Color contour map of current magnitude (in *m*/*s*) for maximum spring ebb tide. Color scale is shown on the right-hand-side. Regions considered "dry" are masked out (based on minimum depths of 0.05 *m*).

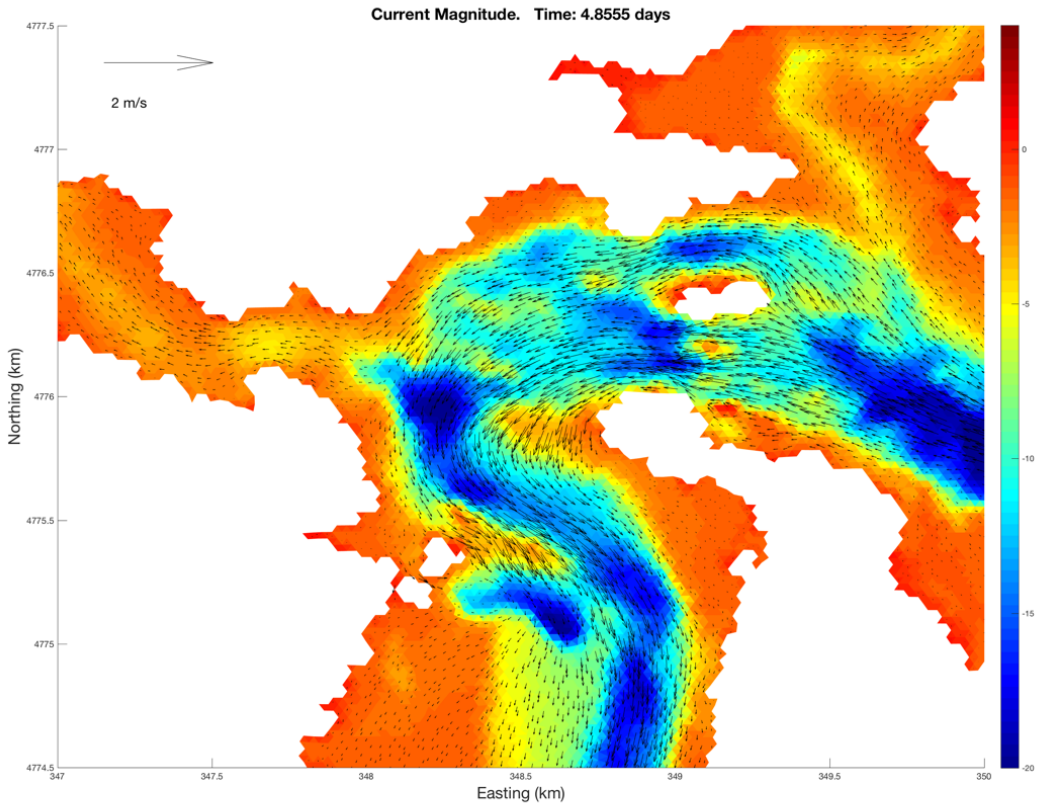

Figure 15. Close-up of flood currents in Little Bay of Great Bay estuary. Only 1/3 of current vectors are shown for display purposes. Vector scale is indicated in the upper left-hand corner. Color contours are water depth relative to mean sea level with scale (in *m*) shown with the color bar on the right-hand-side.

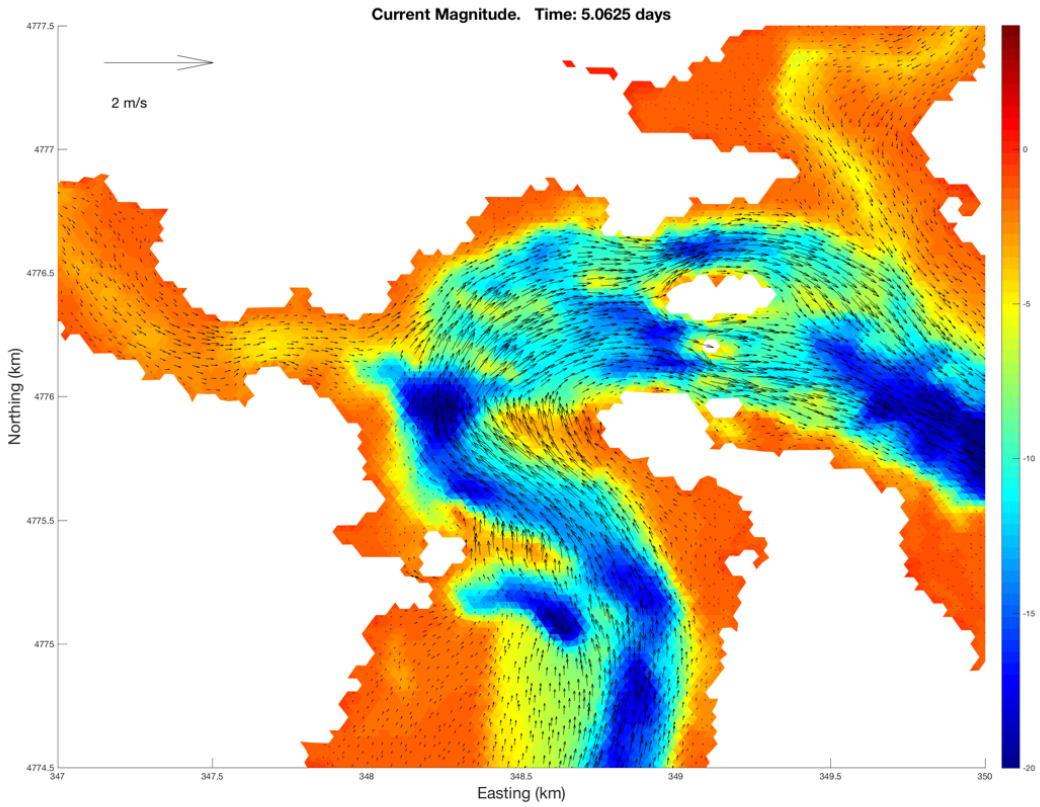

Figure 16. Close-up of ebb currents in Little Bay of Great Bay estuary. Only 1/3 of current vectors are shown for display purposes. Vector scale is indicated in the upper left-hand corner. Color contours are water depth relative to mean sea level with scale (in *m*) shown with the color bar on the right-hand-side.

Tidal Forcing and Subtidal Elevations from 100 Year Tropical Storms (Hurricanes)

FVCOM was run on the 30 *m* grid with tidal plus storm surge prediction from a 100 year flood forcing. The 1.6 *m* storm surge time series (Figure 10) was added to the spring tide in the tidal time series (Figure 11) and used to force the model. This simulation was run without river fluxes owing to difficulties at river boundaries under such large storm surge. The lack of river flux in the model would correspond to very weak fresh water input and is not expected to alter the flooding an inundation results significantly. The maximum ebb currents for this simulation are shown in Figure 17 with the same scale as shown in Figure 14 (for spring tide currents without surge). The current magnitudes are again greatest in the channel and lowest in the upper

estuary and rivers. The highest magnitude is 2.5 *m*/*s*, about 40% higher than the flows without storm surge. Much of the channel from Little Bay to Portsmouth has current magnitude between 1 and 1.5 *m*/*s*, and shows significant increase from typical spring tide conditions.

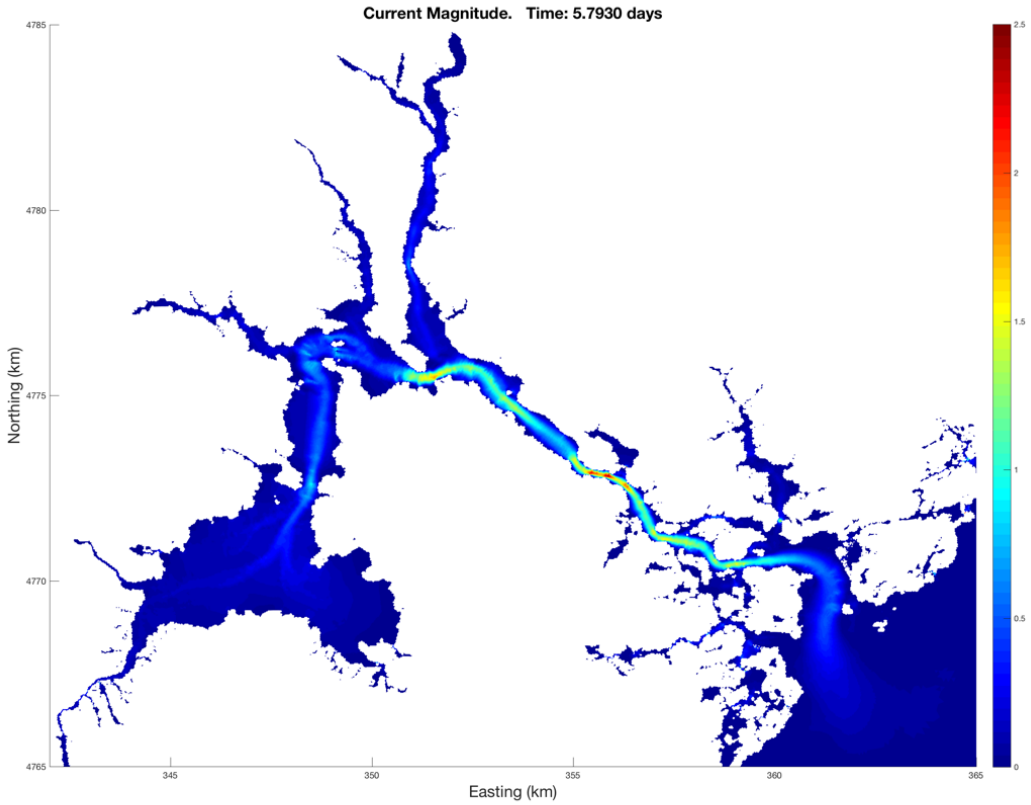

Figure 17. Current magnitude for maximum spring ebb tide with storm forcing.

Tidal Forcing, 100 year subtidal storm, and projected 100 year sea level rise

FVCOM was run on the 30 *m* grid with the aforementioned tidal plus storm forcing time series and with a 2 *m* increase in sea level (obtained from Figure 13). The inundation for the three simulations run for normal spring high tide (SHT), spring tide and storm surge (SHT + SS), and spring tide, storm, and sea level rise (SHT + SS + SLR) are shown in Figure 18 relative to the still water level (MSL). As expected from this initial model simulation, the higher the water level, the more inundation and flooding. The regions that are flooded depend on the elevations and slopes of the topography bordering the water body, as well as the dynamic propagation of

the tides and surge upstream. In particular and of note, the area south of Portsmouth is more severely flooded during both the storm surge and sea level rise scenarios. As well, the upper parts of the estuary near the Squamscott River region is also severely inundated. The Township of Portsmouth and the Portsmouth Naval Shipyard also have increased flooding with increased storm surge and sea level rise scenarios. Some areas with steep river banks do not experience much flooding, but are subjected to significantly increased river flows that could cause accelerated erosion of unconsolidated material.

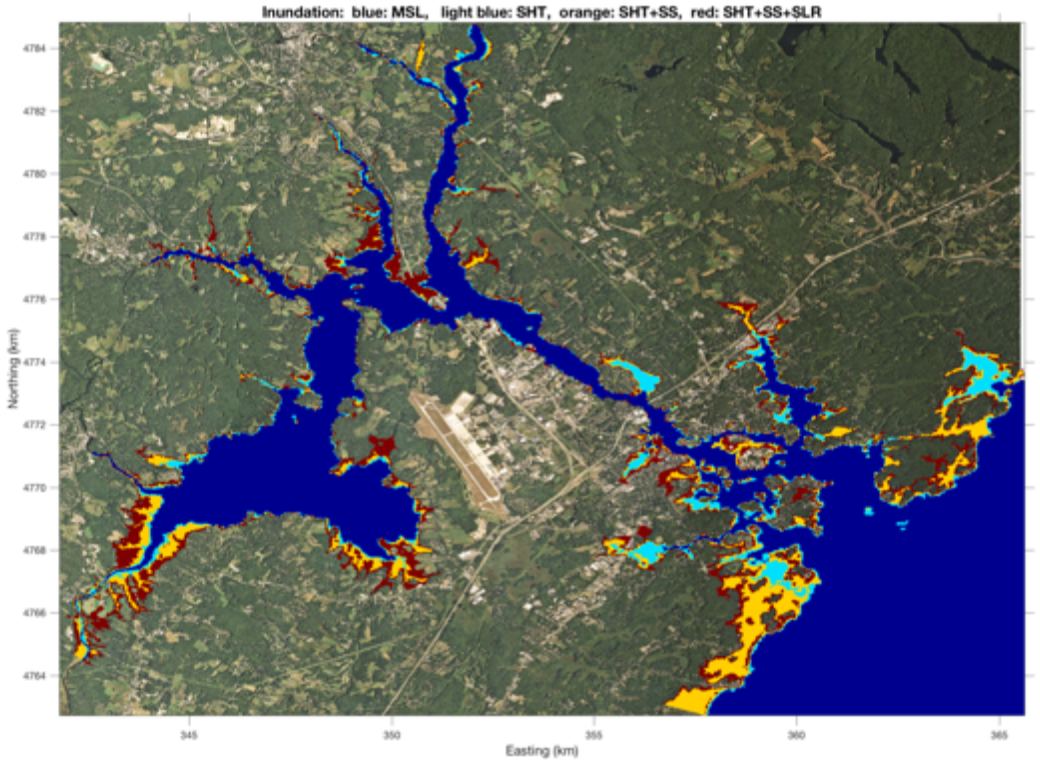

Figure 18. Map of Great Bay estuary with modeled inundation. Blue: mean sea level, light blue: spring high tide, yellow: spring high tide + 100 yr storm surge, red: spring high tide + 100 yr storm surge + sea level rise.

Discussion

The map of flooding and inundation (Figure 18) shows many of the low-lying coastal areas inundated in the storm scenarios. Worst case scenarios were implemented with the storm surge added to the spring tide. Much of coastal New Hampshire would be severely impacted by a predicted 100 year storm in the simulation. Low lying areas of Portsmouth, the Portsmouth Naval Shipyard (PNSY), and Rye experience significant flooding. Increased mean sea level adds further flooding to these areas. The PNSY is bisected during both the 100 year storm surge and in addition to sea level rise scenarios. The area around the Squamscott River is more heavily flooded under increased sea level rise. In general, the areas which are flooded with sea level rise are extended back from the areas without sea level rise.

In flooding and inundation scenarios, the increase in current speeds are also of great interest. Increased current magnitude can create new hazards and effect structures, erosion, and the transport of other constituents. The maximum currents for the normal spring ebb tide (Figure 14) are increased by about 0.70 *m*/*s* or 40% during storm forcing (Figure 17). This added flow greatly increases the bottom stress which scales as the square of the velocity, and the forces on structures that scales as the cube of the velocity. A more quantitative assessment would be needed to more precisely estimate the change in bottom stress and structural forcing.

Limitations to our analysis exist due to the need for more model runs, verification, and statistical analysis. For the storm scenarios, river inputs need to be added. Up to this point, the principal concern has been simulating hydrodynamics under enhance forcing scenarios, without much attention to appropriate mixing parameters. Further analysis of solute transport and mixing would need to be done, and would involve comparisons of observed and modeled salinity and temperature. Additional comparisons with surface drifters or dye studies would also be of great value.

Some man-made structures (*e.g.*, bridges and pilings) around PNSY and other islands in the harbor are unaccounted for. With 30 *m* resolution, these are not well resolved, but are important if the model is utilized to determine potential damage on structures. To better account for these details the grid resolution would need to be refined to about 10 *m* resolution, and then tested in a similar manner as done herein. Simple scaling suggests that the 10 m resolution

would increase the model time by about an order of magnitude, rendering a 10 day run to take about 5 real days of computing time (unless more nodes can be obtained from Trillian).

Ongoing work

This model should be compared with the "bath-tub" model in which everything fills up at to the same level based on static elevation changes at the offshore boundary. This type of model doesn't account for tidal dissipation that occurs in an estuary which lessens the effects of the tides upstream and could lead to overestimation of the flooding scenarios in the upper parts of the estuary. On the other hand, the dynamic behavior of the tides on top of elevated sea level due to storm surge or climate change may offset the tidal energy dissipation.

Another question to consider is where the energy of the flows are distributed as a function of elevation contour. This is important, because of implications for erosion and structural damage in the estuary to neighboring properties, and has great impact on concepts and designs for "green" infrastructure to protect vulnerable areas at risk for erosion.

Conclusions

An unstructured grid with finest resolution equaling 30 *m* was developed for the Great Bay estuary. FVCOM was implemented into Great Bay estuary using this grid, and tested on a 10 day run with river discharges equivalent to 5 times average daily discharge and offshore tidal forcing. The model was tested using the 100 year storm event from NACCS data and with the highest projected sea level rise scenario from NOAA climate change modeling. During both of these scenarios, flooding increases along the coastline. The current magnitude also increases particularly in the narrow channels in the storm and sea level rise scenarios. The initial model results indicate that the grid can be used to model tidal forcing with maximum projected year storm surge and sea level rise in the Great Bay. With further development to include 10 *m* mesh resolution and the inclusion of surface and wind forcing, it may be able to predict future flooding scenarios based on forecasted storm events and sea level rise. This information is valuable to stakeholders in the surrounding communities of Great Bay.

Acknowledgements

I would like to thank Professor Thomas Lippmann for giving me the opportunity to work with him and his group for the past 3 years on various projects and providing me with the guidance and support that I needed to succeed. I would like to thank the other members of this group particularly Salme Cook and Kate Von Krusentein for their encouragement and support over the last year. The Hamel Center for Undergraduate Research, Undergraduate Research Conference, UNH honors program, UNH Earth Science department and Center for Coastal and Ocean Mapping deserve many thanks for providing me support and opportunities to do and present research while at UNH. Thanks to my family for always believing in me and supporting me.

References

Chen, C., Liu, H., Beardsley, R.C., 2003, An Unstructured Grid, Finite-Volume, Three-Dimensional, Primitive Equations Ocean Model: Application to Coastal Ocean and Estuaries. J. Atmos. Ocean. Tech. 20: 159–186.

Chen, C., Beardsley, R.C., Cowles, G., Qi, J., Lai, Z., Gao, G., Stuebe, D., Lieu, H., Xu, Q., Xue, P., Ge, J., Hu, S., Ji, R., Tian, R., Huang, H., Wu, L., Lin, H., Sun, Y., Zhau, L., 2013, FVCOM User Manual Fourth Ed.

Cook, S., and T. C. Lippmann, 2016, Verification of a hydrodynamic model for the Great Bay Estuary, New Hampshire using field data and the Regional Ocean Modeling System (ROMS), *ECM14 Estuarine and Coastal Modeling Conference*, Kingston, RI.

Courant, R., Friedrichs, K., Lewy, H., 1928, Über die partiellen Differenzengleichungen der mathematischen Physik, Mathematische Annalen, (in German), 100 (1): 32–74.

Flather, R.A. and N.S. Heaps. 1975. Tidal Computations for Morecambe Bay. Geophys J. Int., 42: 489-517.

Ip, J.T.C., Lynch, D.R., and C.T. Friedrichs. 1998. Simulation of estuarine flooding and dewatering with application to Great Bay, New Hampshire. Estuarine Coastal and Shelf Science, 47: 119-141

Kobayashi, M.H., Pereira, J.M.C., Pereira, J.C.F. 1999. A conservative finite-volume second-order-accurate projection method of hybrid unstructured grids. J. Comput. Phys., 150: 40-45.

Leendertse, J.J. 1970. A water-quality simulation model for well-mixed estuaries and coastal seas. I: Principles of computation. RM 6230-RC, Rand Corp., New York.

Leendertse, J.J., 1987. A three-dimensional alternating direction implicit model with iterative fourth order dissipative non-linear advection terms. WD-333-NETH, The Netherlands Rijkswaterstaat.

Mellor, G.L. and A.E. Blumberg. 1985. Modeling vertical and horizontal position, productivity and nutrient chemistry of a coastal ocean planktonic food web. Cont. Shelf Res., 13:74-776.

Mellor, G.L., and T. Yamada, 1982. Development of a turbulence closure model for geophysical fluid problem. Rev. Geophys. Space Phys., 20: 851-875.

Persson, P.O. and G. Strang. 2004. A simple mesh generator in MATLAB. SIAM Rev., 46: 329-345.

Plant, N.G., Holand, K.T., and J.A. Puleo. 2002. Analysis of the scale of errors in nearshore bathymetric data. Marine Geology, 191:71-86

Smagorinsky, J. 1963. General Circulation experiments with the primitive equations: The basic experiment. Monthtly Weather Review, 91:99-164

USACE, 2015, North Atlantic Coast Comprehensive Study: Resilient Adaptation to Increasing Risk, Main Report, U.S. Army Corps of Engineers, pp. 216.

Ward, L., Bub, F., 2007, Temporal variability in salinity, temperature, and suspended sediments in the Gulf of Maine estuary (Great Bay estuary, New Hampshire), High Resolution Morphodynamics and Sedimentary Evolution of Estuaries. Ch 7. 151-142

Zheng, L.Y., Chen, C.S., and H.D. Liu. 2003. A modeoing study of the Satilla River estuary, Georgia. I: Flooding-drying process and water exchange over the salt marsh-estuary-shelf complex. Estuaries, 26: 651-669